JOURNAL OF MATERIALS SCIENCE 29 (1994) 1786–1794

Microscopy investigation on fracture mechanisms in hot-isostatically pressed Si_3N_4/SiC-platelet composites

G. PEZZOTTI
The Institute of Scientific and Industrial Research, ISIR, Osaka University, Ibaraki 567 Osaka, Japan

B.-T. LEE, K. HIRAGA
Institute for Materials Research, Tohoku University, Katahira, Aoba-ku, Sendai 980, Japan

T. NISHIDA
Kyoto Institute of Technology, Faculty of Polytechnique Science, Department of Materials Engineering, Matsugasaki, Sakyo-ku, Kyoto 606, Japan

Fracture mechanisms in hot-isostatically pressed (HIP) Si_3N_4/SiC-platelet composites have been investigated by transmission electron (TEM) and scanning electron (SEM) microscopy followed by profilometric analyses. Two composites containing 25 vol% platelets were compared. They were fabricated from the same raw materials and by the same procedure except for the cooling rate from the sintering temperature. The study consists of experimental observations as well as measurements of fractographic parameters which dictates the level of toughening, such as the percentage of intergranular fracture, lengths and angles associated with the debonding process at the matrix/platelet interface. The presence of microcracking in the neighbourhood of the main crack, a higher fraction of intergranular fracture, as well as substantial debonding at the nitride/carbide interface up to high orientation angles were found in the composite cooled at low rates ($\sim 100\,^{\circ}C\,h^{-1}$) which, despite the unchanged microstructure, was substantially tougher than that cooled at $\sim 650\,^{\circ}C\,h^{-1}$. These trends were not observed in the composite subjected to fast cooling. The stronger interfacial bonding found after fast cooling under high pressure was attributed to an apparent compressive stress remaining stored at the grain boundary, rather than to a weakening of the platelets or the matrix grains. Calculations based on the mechanics analysis of crack/interface interactions and on quantitative profilometric data, indicated a difference of about one order of magnitude in the apparent interface fracture energy of the two composites.

1. Introduction

Fracture behaviour of ceramic composites is a rather individual phenomenon depending complexly upon many subtle microstructural circumstances which have not been fully understood and rationalized. One of the major difficulties in fracture analysis of ceramic composites is that the characteristic length scale of the fracture phenomenon may range over several orders of magnitude. Accordingly, analyses should be attempted monitoring the material by various complementary techniques. Fracture mechanics tests which can provide precise quantitative data on the macroscopic fracture resistance of the composite, necessarily need to be coupled with microscopic observations of the crack path in order to aquire insight into the fracture process and to optimize it by iterative experiments.

Recent studies on whisker-reinforced composites [1, 2] have demonstrated the importance of TEM characterizations of the crack path for understanding the micromechanics of fracture in ceramic composites. Rather than *in situ* experiments, whose results can be strongly affected by thin-foil effects on the microfracture mode, a crack of appropriate dimensions can be first introduced by a Vickers indentation on a thick sample from which a thin foil is successively obtained by a back-thinning procedure. This method permits minimization of the effect of extraneous phenomena and observation of the original crack extent. However, TEM experiments allow the observation of an area around (especially behind the crack tip) which can be very limited compared with the characteristic length of the fracture phenomenon. Depending on the fraction, geometry and micromechanical characteristics of the reinforcing phase, the wake-zone behind the crack tip which is still operative in energy dissipation, can vary from micrometre to millimetre scale. Consequently, although TEM observation may be the only tool

0022–2461

to analyse in detail the near-tip phenomena, it needs to be integrated with more conventional fractographic techniques giving information on a larger scale. In the present study, the near-tip micromechanisms of fracture in a SiC-platelet-reinforced Si_3N_4 system were analysed by the back-thinning TEM technique. In addition, in accordance with previous studies [3, 4] indicating a characteristic wake-zone length about one order of magnitude larger than the observable dimension of the TEM sample, a detailed profilometric analysis of the fracture surfaces by a three-dimensional scanning image analyser (3D SIA) was employed for a complementary analysis of the crack–microstructure interactions.

2. Background on HIPed Si_3N_4/SiC-platelet composites

In a previous report [3], a phenomenological analysis of fracture behaviour was presented for a series of Si_3N_4/SiC-platelet composites sintered by glass-capsule HIPing without external addition of additives [4]. All the materials were fully dense (> 99.5%) after 1 h sintering at 2050 °C under 180 MPa isostatic pressure. The dependence of macroscopic fracture properties on material compositional and processing parameters such as the volume fraction of platelets, cooling-rate from HIPing temperature, applied pressure and annealing temperature, was systematically monitored and quantitatively related to the morphology of the fracture surface through a 3D SIA technique.

The cooling-rate from the HIPing temperature was indicated to be a critical parameter when cooling was performed under high pressure. Despite the unchanged morphology of the glassy-SiO_2 grain-boundary, and the Si_3N_4 grains having essentially the same size [5] with varying cooling rate, a marked embrittlement of the composite body was found for fast cooling ($\sim 650\,^{\circ}C\,h^{-1}$), while the highest fracture resistance and work of fracture (WOF) were obtained with cooling at $\sim 100\,^{\circ}C\,h^{-1}$. From a phenomenologic point of view, the embrittlement was represented by a decrease in roughness of the fracture surface and in the observed debonding length of the platelets, as quantitatively specified by automatically scanning a large series of fracture profiles. Because no spontaneous microcracking was detected by TEM under any cooling conditions investigated and because systematic annealing experiments carried out in nitrogen atmosphere up to 1750 °C (i.e. up to temperatures higher than the melting point of the glassy SiO_2 grain boundary) also demonstrated that the composite fracture properties were almost unaffected by the cooling rate in the absence of high applied pressure, it was hypothesized that the severe embrittlement was induced by micromechanical residual stresses thermomechanically related to the HIPing schedule. In this work, we examined by TEM the microfracture modes of two of the above series of Si_3N_4/SiC-platelet composites both containing 25 vol % reinforcing phase. The 3D SIA data are re-examined with respect to the platelet orientation rather than in terms of surface roughness.

Quantitative image analysis demonstrated [5, 6] that in the present composites: (1) the platelets (Grade M, C-Axis Technology, Jonquiere, Canada) after sintering have average diameter, $\bar{D}$, and thickness, $\bar{t}$, of 22.6 μm and 3.2 μm, respectively, (2) the platelets are embedded in the matrix with a high degree of three-dimensional randomness, and (3) the added SiC volume fraction leads to an average centre-to-centre near-neighbours distance, $\bar{\Delta}$, of 32.7 μm. The composites were, respectively, cooled after HIPing at 650 and $100\,^{\circ}C\,h^{-1}$, and showed markedly different fracture behaviour, the latter (composite A) being substantially tougher than the former (composite B). The fracture mechanics data relative to these two composites are summarized in Table I in comparison with those of the Si_3N_4 matrix (E10, Ube Industries, Ube, Japan) sintered by a similar HIPing schedule [4, 7]. In Table I, roughness data by 3D SIA from Pezzotti *et al* [3] are also summarized.

3. Microscopy results

3.1. Transmission electron microscopy

Observations of the microfracture mode of Si_3N_4 grains and of the crack/SiC-platelet interaction have been made using TEM. Before any further discussion, it should be emphasized that, differently from the case of whisker composites [1, 2] and due to the geometrical characteristics of the present SiC phase, neither the mechanical dimpling nor the successive ion-thinning procedure in the region of the indentation crack tip could be limited to a thickness in excess of the average half-diameter of the SiC platelets (i.e. > 11 μm). Although, however, the back mechanical thinning was performed only by a long and light polishing procedure, a certain degree of uncertainty may remain about whether the observed debonding length at the platelet/matrix interface represents the actual behaviour in the bulk material or it was somehow altered by extrinsic factors related to the preparation of the TEM sample. Because we could not resolve this problem in the present investigation, debonding length data from TEM images will not be quantitatively discussed hereafter.

Two basic differences between composites A and B were recognized by TEM analysis. They are: (1) the high percentage of intergranular fracture of the Si_3N_4 matrix in composite A contrary to its almost completely transgranular fracture mode in composite B,

TABLE I Fracture properties of HIPed monolithic Si_3N_4, and Si_3N_4/SiC-platelet composite A and B. K_{Ic}, K_R^{max}, WOF and R_L are the fracture toughness, the asymptotic toughness (i.e. the maximum value measured by *R*-curve experiment), the work of fracture and the profile roughness, respectively. The measuring unit-length adopted in the roughness measurement was 0.6 μm [3]. (Fracture mechanics data are obtained by chevron notch technique in bending. Experimental details are reported elsewhere [3, 8])

	K_{Ic} ($MP\sigma\,m^{1/2}$)	K_R^{max} ($MP\sigma\,m^{1/2}$)	WOF ($J\,m^{-2}$)	R_L
Monolithic	2.4	2.4	10.7	1.04
Composite A	4.9	⩾ 9.0	58.6	1.34
Composite B	4.0	4.5	43.3	1.26

Figure 1 Typical crack path observed by TEM in composite A with a high percentage of intergranular fracture in the Si_3N_4 matrix and debonding at the carbide interface. The crack propagation direction is arrowed. Small arrows indicate microcracking.

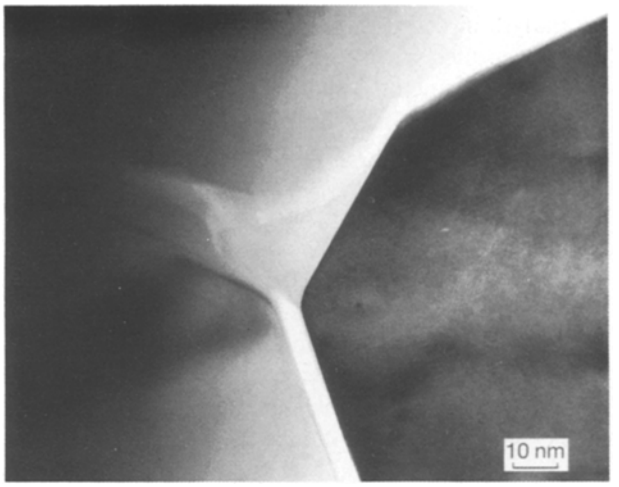

Figure 2 High-magnification TEM image of a microcrack at the matrix grain boundary. The glassy-SiO_2 triple junction and intergranular film are seen to be fractured, while the Si_3N_4 grains remained intact.

Figure 3 Near-tip region in composite B observed by TEM. The crack tip is arrowed.

and (2) the presence of microcracking sited at some Si_3N_4/Si_3N_4 grain boundaries close to the crack path in composite A which were not observed in composite B. Notice that both these phenomena should be of the bulk materials proper and not affected by the sample preparation procedure, because both the TEM samples were prepared by the same procedure and their thickness was comparable with the average size of the Si_3N_4 grains in both the composites.

Fig. 1 shows the typical crack path observed by TEM in composite A. As seen, the main crack path proceeded almost completely intergranularly between the equiaxed Si_3N_4 grains whose average size was measured as ~ 1 μm. It was generally observed that the crack debonded along the Si_3N_4/SiC interface even at high relative angle between the main crack direction and the platelet axis (in Fig. 1 the relative angle is nearly 90°). Tilting studies have also revealed the presence of microcracking sited near the crack path in composite A. They are indicated by arrows in Fig. 1. Microcracks were generally located at the grain boundary and they were observed up to distances of several grain diameters from the main crack. It is also noted that microcracks were usually originated at the glassy-SiO_2 triple junctions between grains, as better shown in the high-magnification TEM image of Fig. 2. A high percentage of transgranular fracture was instead observed in composite B. Fig. 3 shows a near-tip zone in composite B. The high stress at the crack tip (indicated by an arrow) is manifested in the strain fringes around it. No systematic presence of microcracking was observed in this material after extensive tilting experiments. Higher magnification images of crack propagation in composite A documented the occurrence of frictional phenomena in the crack wake along the grain boundary of the matrix as shown in Fig. 4a. On the other hand, some limited debonding at the matrix interface was revealed by more detailed observation in sites contiguous to the transgranular path in composite B (cf. arrowed boundary in Fig. 4b). The comparison between Figs 1, 3 and 4 also confirms that no obvious difference can be found in the size and morphology of the microstructural features in composites A and B. Slightly kinked propagation, which

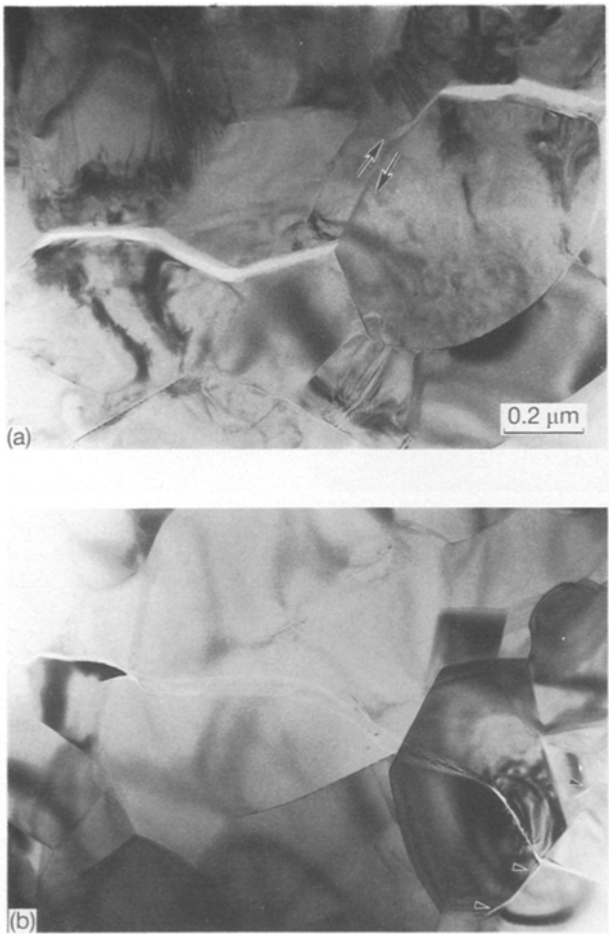

Figure 4 Details of matrix fracture observed by TEM. (a) Intergranular propagation with friction between adjacent grains in composite A. (b) Transgranular kinked propagation in composite B. Arrows in (b) indicate some crack splitting at the grain boundary, occasionally observed in the immediate neighbourhood of the main path in composite B.

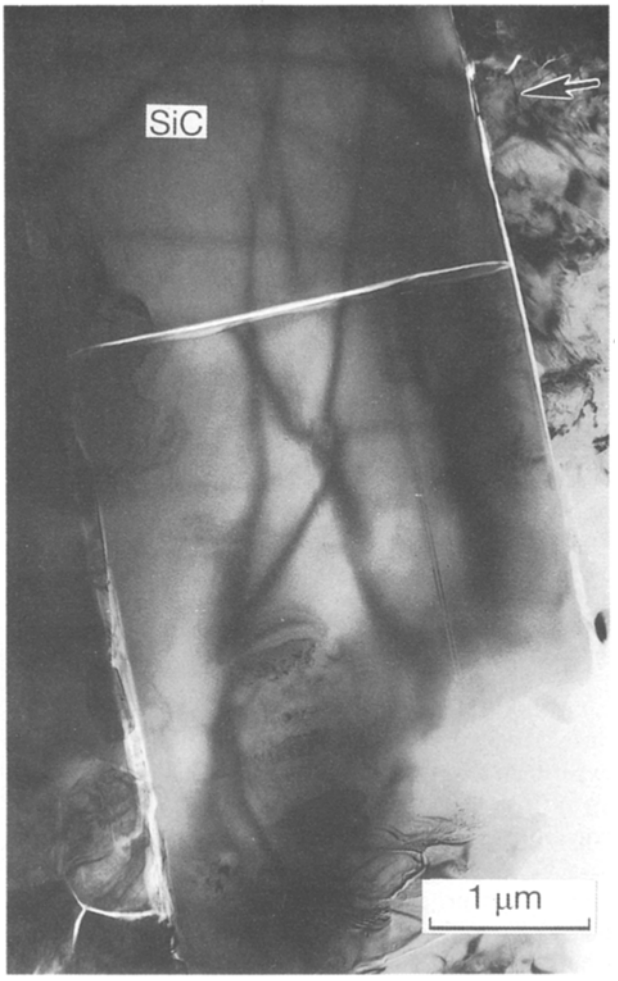

Figure 5 Details of the crack/platelet interaction observed by TEM. The arrow indicates the main crack direction.

often occurred inside the Si_3N_4 grains (Fig. 4b), may be related to the presence of residual stresses in the matrix after the HIPing process in composite B. Because an extent of crack path about two orders of magnitude larger than the grain size of the matrix could be analysed in detail by TEM; a reliable estimate of the percentage of intergranular fracture could be obtained for both the composites under investigation. We measured 71% matrix grain-boundary propagation in composite A compared with only 8% in composite B.

The interaction between crack and SiC platelets was also investigated in some detail although only qualitatively by TEM. Fig. 5 shows the typical case of a platelet oriented at $\sim 90°$ with respect to the main crack (arrowed). The sequence of microfracture events can be deduced as follows: when the main crack first interacted with the platelet, the interface debonded to a length larger than the platelet thickness. The platelet which generally has a large lateral extent, is not easily circumvented nor surrounded by the propagating crack. Therefore, it is most likely that, being loaded in tension (and bending for orientation angles $< 90°$), it cleaved successively, leading to debonding at the opposite interface and further crack propagation from a stress accumulation point at this latter debonded boundary. Note that the cleavage plane, whose only trace is visible in the TEM profile, is not necessarily parallel to the main crack plane. Intact platelets were not observed, even in the immediate neighbourhood of the crack tip. In other words, no evidence of a bridging zone could be provided by TEM observation.

Some interesting details could be recognized by observing at high magnification the region near to the debonded Si_3N_4/SiC boundary (Fig. 6). First, it was found that the platelet boundaries were interlocked with the Si_3N_4 grains: a micromechanical circumstance which may play an important role during the fracture phenomenon. It is clear that such interlocking can markedly enhance the roughness of the interface and inhibit the occurrence of large pull-out extents. This point will be discussed in some detail below in relation to quantitative fractographic data. It should be noted here that, following the complementary profiles of the matrix grains and the SiC platelet, as for example in Fig. 6, the shift of points originally coincident can give a direct measure of the pull-out length before platelet fracture. In the present system, a complete pull-out of an intact platelet was rarely observed (see next section). Platelets fractured within a pull-out extent typically < 400 nm.

Another interesting finding is concerned with the internal structure of the Si_3N_4 grains in the neighbourhood of the SiC platelets. Quite a high density of

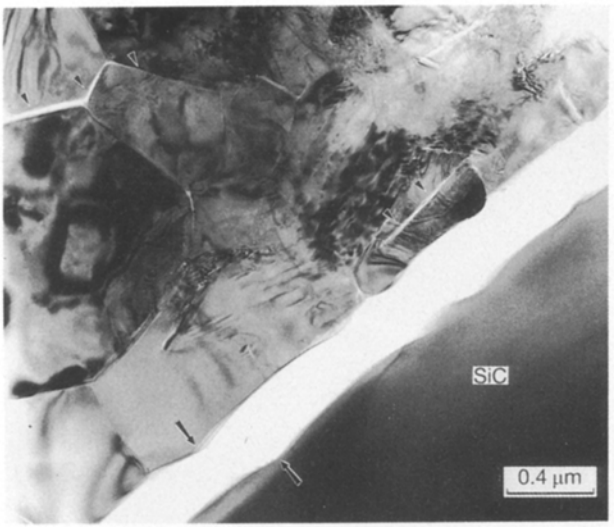

Figure 6 TEM image of a region close to a fractured nitride/carbide interface in composite A. High dislocation density is noted in the matrix grains. Microcracks (small arrows) are observed both at the grain boundary and inside the matrix grains. Large arrows indicate interface points originally coincident prior to fracture.

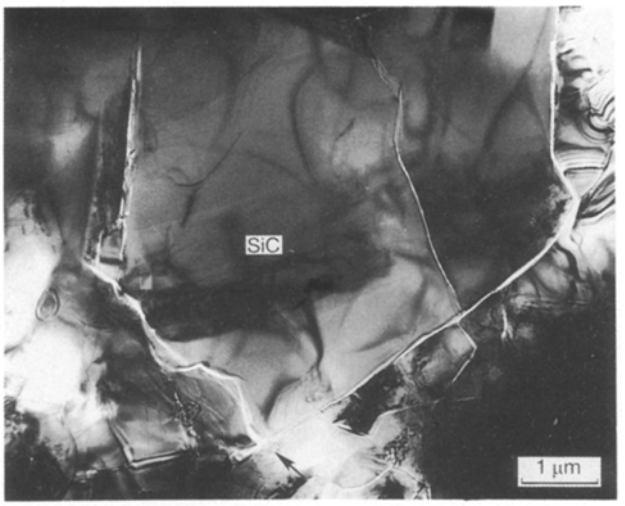

Figure 7 TEM observation of the complex crack/platelet interaction in the case of the diametrical plane of a platelet aligned with the crack profile. The arrow indicates the direction of the main crack path.

dislocations was observed in these grains by tilting experiments in comparison with grains in regions far away from the SiC phase. In some grains, internal cracking was also observed (Fig. 6). This phenomenon may be somehow related to the mismatch in thermal and elastic properties between nitride and carbide phases, as well as to the HIPing schedule. However, whether or not this circumstance leads to an easier debonding is a fact of difficult interpretation and cannot be unambiguously substantiated with the present investigation.

The crack/platelet interaction appeared to be very complex for platelets oriented with the diametral faces aligned with the propagation direction of the main crack as shown in Fig. 7. The platelet/matrix boundary was as often as not completely debonded and extensive internal cracking was observed in the platelets. The origin of the secondary cracks inside the SiC phase was different from the cleavage path and they also developed kinks and branches, suggesting complex interactions with the platelet crystal structure. Such an observation is in agreement with the characterization by SEM presented in Section 3.2. No distinction has been made between composites A and B in the above description of the crack/platelet interaction, because in this study we could not identify any definite difference between these two materials on the TEM scale.

3.2. Scanning electron microscopy and profilometric analysis

The 3D SIA represents a very powerful fractographic technique by which it is possible to analyse automatically and in detail large areas of fracture surfaces. Although also scanning at high magnification is possible, however, some characteristics of the microfracture behaviour of the material, such as microcracking at the matrix grain boundary, debonding beyond the pulled-out portion and internal cracking of platelets

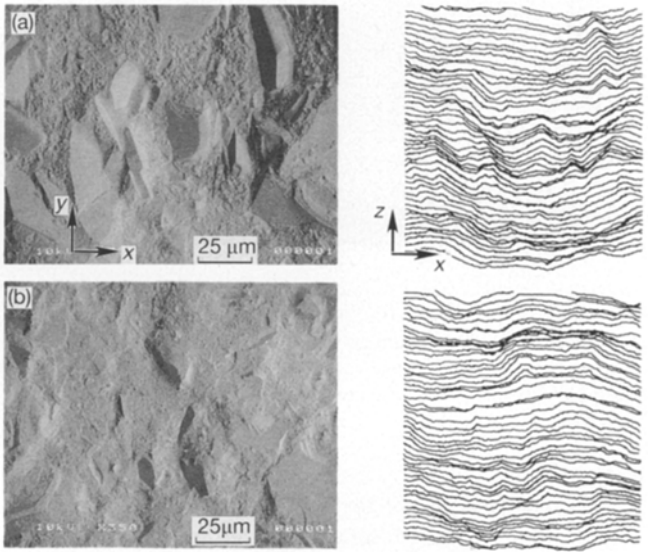

Figure 8 Low-magnification SEM images of fracture surfaces and relative 3D SIA profilometric analyses giving an overview of the fracture in (a) composite A and (b) composite B. Crack propagation is in the direction of the x-axis.

which may occur inside the specimen, are not detectable. This technique can be considered complementary to TEM analysis because it provides a complete look over the fracture phenomenon. In this study, we analysed the entire fracture surface of composite specimens after fracture mechanics test whose results are summarized in Table I. Because the complete description of the mechanical testing procedure and the SEM images of the fracture surfaces with relative 3D SIA profiles were reported previously [3] (cf. roughness data in Table I), only details about the crack/platelet interaction will be discussed hereafter. The fracture surfaces of composites A and B examined within the spatial resolution of the SEM (Fig. 8a and b, respectively) show quite different morphological characteristics, the observed pull-out length of the SiC platelets being more pronounced in composite A. In Fig. 8, the respective 3D profilometric analyses are

also represented. Depending upon the relative orientation between crack and platelet, as well as the crystallographic orientation of the platelet, a wide range of different microfracture behaviour has been observed. The salient cases for composite A are summarized in Fig. 9a–c in which the respective three-dimensional profiles are also drawn. When the platelet main plane was oriented at about 90° with respect to the fracture plane, either cleavage or sawtooth fracture mode could occur (Fig. 9a and b, respectively). The cleavage plane was generally parallel to the platelet thickness and, according to the orientation angle, a portion of the debonded interface was observed. Fig. 9a shows the typical case of a large SiC platelet oriented at a high angle ($\sim 70°$) on the main fracture plane which cleaved without apparent debonding along the first interface. The profilometric analysis performed along the line indicated by arrows in the scanning electron micrograph, showed a significant debonded portion (27.2 μm long) at the successive platelet/matrix interface. Sawtooth fracture occurred when the cleavage plane of the platelet was markedly misaligned respect

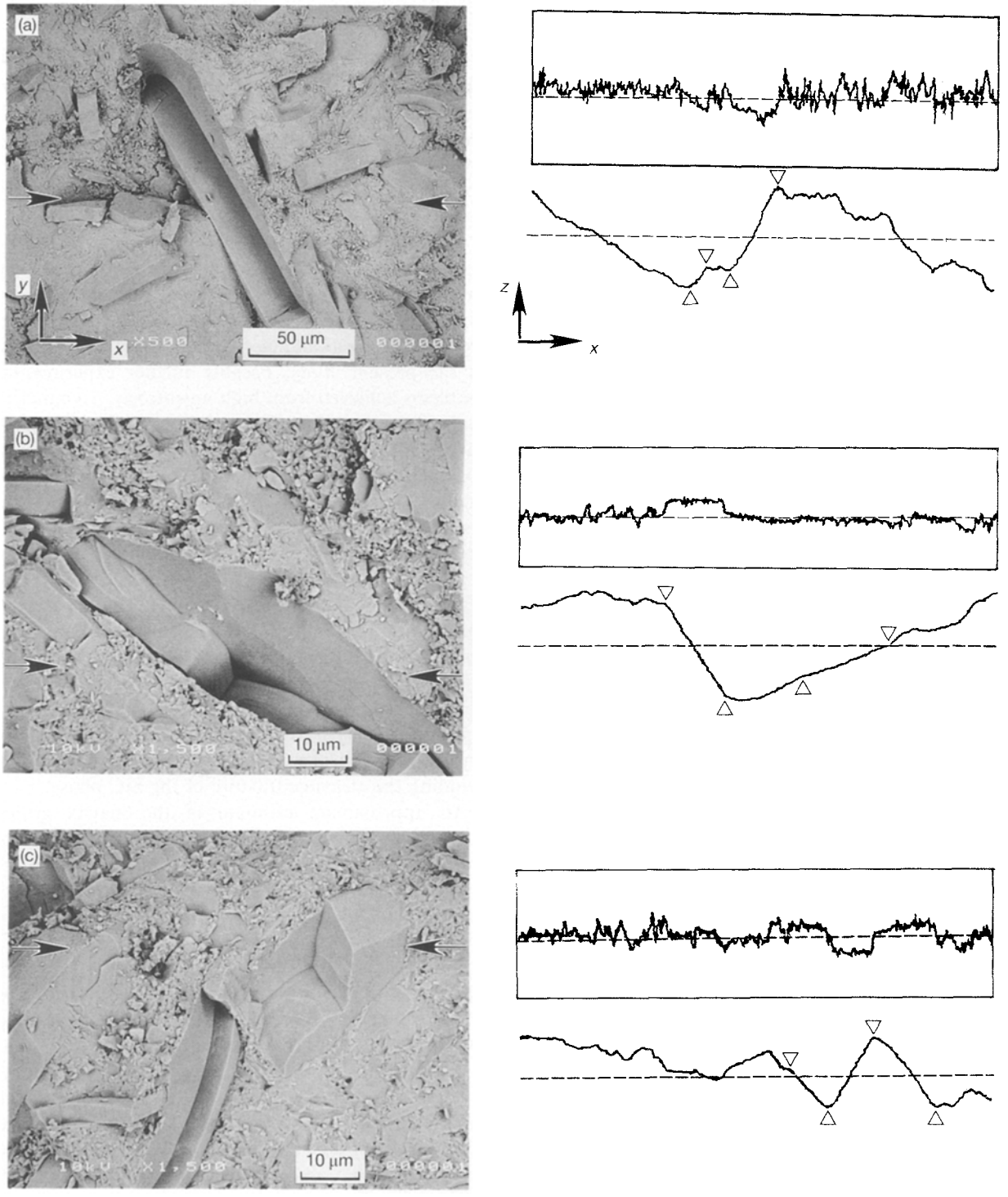

Figure 9 Back-scattered SEM images and relative 3D SIA data for the crack/platelet interaction in composite A. The analyses have been performed along the profile indicated by arrows. For completeness, the differential brightness profiles from which the lengths along the z-axis have been calculated, are also shown (upper thick profiles). The crack propagated in the direction of the x-axis. Open arrows delimit segments of the nitride/carbide interface opened by the crack.

to the main fracture plane. In Fig. 9b this latter case is represented. Owing to the higher fracture resistance of the SiC crystallographic plane intercepted by the crack, the main path was tilted out along the matrix/platelet interface. The microfracture sequence in this case might be similar to that described for Fig. 5. The observed debonding length was measured as 10.6 μm at ~ 66°. Fig. 9c shows one of the quite complex patterns observed when the platelets had the faces almost aligned with the crack profile. These cases are difficult to interpret owing to the highly anisotropic fracture properties of the platelets and the complex stress field to which they are subjected. Composite B showed a much higher number of cleavage fractures. Although the observed portions of interface subjected to debonding were generally more limited compared with composite A, the microfracture mechanisms appeared to be similar to that above described.

Based on the precise quantitative determination by 3D SIA of angles and lengths associated with the interface debonding and the pull-out process of the SiC phase, a statistical analysis was attempted by screening a large number of profiles in the fracture surfaces of composites A and B. According to microstructural data obtained by image analysis [5, 6], it was estimated that the analysed number of platelets constituted a significant fraction which can be representative of the total number of platelets encountered by the main crack plane. (Twenty profiles per each chevron-notched specimen were analysed leading to a total investigated profile length of ~ 12.8 mm. Because the average centre-to-centre near-neighbours distance was 32.7 μm, the total number of platelets investigated for each material was ~ 390 which represents ~ 1/6 of the total number of platelets encountered by the main fracture plane during the chevron notch experiment [3, 5].) In the analysis, length and angles associated with the crack path were counted on profiles whose scale was the same as that shown in Fig. 9. In other words, the analysis was performed on the scale of the SiC-platelet length neglecting the segments associated with the Si_3N_4 grains, which were generally more than one order of magnitude smaller (cf. Fig. 9). The results of this analysis are summarized in the histograms of Fig. 10 in terms of fractional length which represents the fraction of the total profile length oriented at each angle (corresponding to $5j + 2.5°$ with $j = 0, 1, 2, \ldots$).

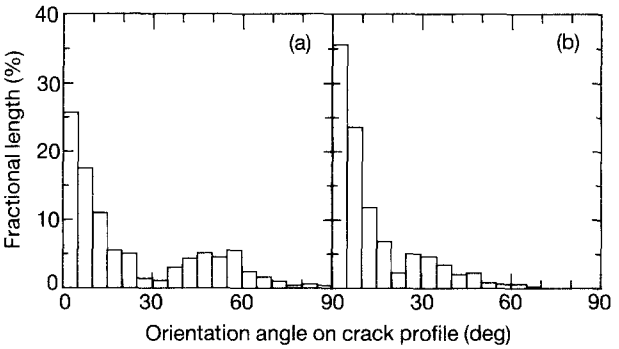

Figure 10 Histograms of fractional length summarizing the 3D SIA data for composites (a) A and (b) B.

4. Discussion

4.1. Crack/matrix-grain interaction

Composites A and B, despite their identical phase composition and microstructural morphology, showed quite different fracture behaviour over a wide range of observation scales. Submicrometre analysis by TEM (Figs 1 and 2) revealed the presence of grain-boundary microcracking in the neighbourhood of the main crack, as well as a large fraction of intergranular fracture mode of the matrix only in the tougher composite A. Moreover, stereoscopic fractography by SEM on the characteristic scale length of the SiC platelets (i.e. 10 μm scale) showed (Figs 8–10) a quite higher length of interfacial debonding in composite A whatever the relative angle between platelet and main crack path, compared with composite B (Fig. 10). All these circumstances actually prove that the strength of the Si_3N_4/Si_3N_4 as well as that of the Si_3N_4/SiC boundaries were lower in composite A than in composite B.

A quantitative analysis of the microcracking phenomenon from TEM data has been attempted by Ruhle [9] for oxide ceramics. It was shown that experimental microcrack detectability limitation in the TEM severely hampers quantitative conclusions. In the present study, because further experimental problems achieved from high anisotropy, asymmetric shape and large dimensions of the SiC platelets compared with the thin TEM foil, a similar evaluation was not attempted. Besides its uncertain contribution as a toughening mechanism itself in the present composite system, however, it is clear from the comparison between composites A and B that microcracking plays a key role as a precursor mechanism for successive crack bridging and pull-out mechanisms. In accordance with the understanding that some debonding is generally needed to eliminate the singularity when the matrix crack intercepts the platelet [10], the presence of an opened portion of interface ahead of the advancing crack front (i.e. the nucleation of a grain-boundary microcrack) becomes a necessary condition for avoiding the cleavage fracture of the SiC phase.

An approximate estimate of the matrix grain-boundary fracture energy, γ_{gb}, of polycrystalline ceramics can be obtained from the fraction of intergranular fracture, ξ, according to the following equation [11]

$$\gamma_{gb} = (E'_m/E'_{gb})\gamma_m \cos^4(\xi\pi/2) \quad (1)$$

where $E' = E/(1 - \nu^2)$ is the elastic modulus for the plane strain conditions, ν is the Poisson's ratio and the subscripts m and gb refer to matrix grains and grain boundary, respectively. Because the ξ values of composites A and B were precisely measured by TEM experiments, and the other parameters involved are known, being previously measured or available in the literature, Equation 1 can be applied to the matrix microstructures of the present composites. For E_m, ν_m and γ_m equal to 312 GPa, 0.23 [12] and 10.7 $J\,m^{-2}$ [8], respectively, and $E_{gb} = 72$ GPa and $\nu_{gb} = 0.16$ (values for SiO_2 glass [13]), the fracture energies of the

matrix grain boundary of composites A ($\xi = 0.71$) and B ($\xi = 0.08$) are respectively, calculated from Equation 1 as $\gamma_{gb}^{A} = 2.0\,J\,m^{-2}$ and $\gamma_{gb}^{B} = 46.1\,J\,m^{-2}$. This calculation, although approximate, suggests that a non-negligible compressive residual stress remains stored at the Si_3N_4/Si_3N_4 grain boundary after fast cooling under the high isostatic pressure. Note that in composite A, γ_{gb} is close to the fracture energy of SiO_2 glass, a fact suggesting that such stress can be controlled by appropriately scheduling the HIP cycle. Considering that the two composites have the same morphology of matrix grains and grain boundaries as well as the same Young's modulus, it can be demonstrated [14] that for a polycrystalline aggregate of hexagonal grains

$$\sigma_c^A/\sigma_c^B \simeq (\gamma_{gb}^A/\gamma_{gb}^B)^{1/2} \quad (2)$$

where σ_c^A and σ_c^B are the interface compressive residual stresses in composites A and B, respectively. Equation 2 leads to the indicative result in terms of residual stresses $\sigma_c^A \simeq 0.2\,\sigma_c^B$.

4.2. Crack/platelet interaction

A low fracture resistance interface exists with interfaces subjected to residual tension, leading to partial debonding in advance of the crack tip or, in some limiting cases, during cooling from the sintering temperature. Rigorous elastic solutions of the stress field around platelet-shaped inclusions, also including the effect of anisotropy in elastic constants and thermal expansion coefficients, are available [15, 16] and have been recently worked out for Si_3N_4/SiC composites [17]. They show that, consistent with the higher thermal expansion of the SiC phase compared with that of the Si_3N_4 matrix, a residually stressed matrix/reinforcement interface in tension should be developed after sintering. However, although these calculations can be somehow indicative also in the present HIPed system, they cannot be applied directly. According to the elastic stress field solution (i.e. neglecting any time-dependent phenomenon during cooling), the two present composites should have exactly the same fracture behaviour.

In addition to the complexity of the micromechanics of the platelet fracture whose solution obviously depends upon the concurrent action of creep under the high isostatic pressure and temperature of the SiC single crystals and their thermal and elastic mismatches with the Si_3N_4 matrix, some rationale about the fracture process in the present composites can be obtained by taking into account the statistical profilometric data of Fig. 10 and the mechanics of a crack impinging the interface between two dissimilar materials [18–21].

For a semi-infinite crack proceeding perpendicular to the Si_3N_4/SiC interface the relative tendency of a crack to be deflected by the interface rather than to pass through it, can be assessed using the following condition [21]

$$G_{ic}/G_c < G_d/G_p = [(1 - \beta^2)/(1 - \alpha)][|d|^2 + |e|^2 + 2R_e(de)]/c^2 = \delta \quad (3)$$

where G_d and G_p are the strain energy release of the crack deflected at the interface, and that for straight penetration in the SiC phase, respectively. G_{ic} and G_c are the toughness of the interface and that of the matrix, respectively. The Dundurs' parameters, α and β, are given [22] as a function of the elastic constants of the two materials as

$$\alpha = [\mu_c(1 - \nu_n) - \mu_n(1 - \nu_c)]/[\mu_c(1 - \nu_n) + \mu_n(1 - \nu_c)] \quad (4)$$

$$\beta = [\mu_c(1 - 2\nu_n) - \mu_n(1 - 2\nu_c)]/[\mu_c(1 - \nu_n) + \mu_n(1 - \nu_c)] \quad (5)$$

where μ is the shear modulus and the subscripts c and n refer to the carbide and nitride phase, respectively. The parameters c, d and e are complex valued functions of the adimensional Dundurs' parameters and δ is a real adimensional coefficient which have been calculated by He and Hutchinson [21] for homogeneous materials. Neglecting the anisotropy and the finite thickness and diameter of the carbide phase in the present composites, as well as considering the dependence of the above complex functions on β to be negligible (i.e. $\beta = 0$) [21, 22], an estimate of the interface fracture energy can be obtained from Equation 3. The present approach is similar to that adopted recently by Bhattacharya *et al.* [23] to discuss the fracture energy of a wedge-loaded crack impinging a Si_3N_4/SiC interface. Note that Equation 3 is independent of the debonding length, a decisive fact for its applicability to the present experiments. In composite A, interface debonding could be systematically observed for platelets oriented at 90° on the main fracture plane. On the other hand, depending upon the crystallographic orientation of the platelet (i.e. for orientation angles $> 60°$, from Fig. 10) straight fracture at the crack tip through the carbide phase was found in composite B. These observations allow estimation from Equation 3 of the interface fracture energy of the composites. Introducing the known elastic parameters for the nitride and carbide phases ($\alpha = 0.75$) and the numerical results from He and Hutchinson [21], the values $\delta = 0.83$ and $\simeq 1$ are found from the right-hand side of Equation 3 for composites A and B, respectively. This leads to the following limiting conditions

$$\gamma_i^A < 0.83\,\gamma_{cl} \quad (6)$$

$$\gamma_i^B > \bar{\gamma} \quad (7)$$

where γ_i^A and γ_i^B are the fracture energies of the platelet/matrix interface in composites A and B, respectively, and $\gamma_{cl} = 3.15\,J\,m^{-2}$ [24] and $\bar{\gamma} = 8.8\,J\,m^{-2}$ [25] represents the cleavage fracture energy of the platelet and the fracture energy of SiC averaged over all the possible crystallographic directions, respectively. Similar to the matrix behaviour, this calculation indicates that also at the nitride/carbide interface in composite A the apparent fracture energy is about half that of SiO_2 glass and more than four times smaller than that in composite B. Invoking again the similarity in morphology and phase composition of these two composites, it is again found that

a non-negligible apparent compressive interface stress remains stored in HIPed Si_3N_4/SiC composites cooled at fast rates under high pressure.

5. Conclusion

The fracture modes of two Si_3N_4/SiC-platelet composites have been investigated by TEM and SEM followed by quantitative profilometric analysis. Both the composites contained 25 vol % platelets and were fabricated by the same HIPing schedule, except for the cooling rate. Despite their very similar microstructural characteristics, such as the size and morphology of the matrix grains and that of the glassy-SiO_2 grain boundary, these two composites showed substantially different toughnesses. The presence of microcracking at the matrix grain boundary in the neighbourhood of the main crack path, as well as a markedly higher percentage of intergranular fracture, led to higher toughness and revealed a weaker interfacial bonding in composite A cooled at a slow rate ($\sim 100\,^{\circ}C\,h^{-1}$) compared with composite B fabricated at $\sim 650\,^{\circ}C\,h^{-1}$. Attributing the differences in the microfracture mode of these two composites entirely to a residual compressive stress stored at the grain boundary during fast cooling under high pressure and in accordance with quantitative profilometric data, the apparent fracture energy of the interfaces in composite A has been estimated to be about half that of SiO_2 glass and about one order of magnitude smaller than that in composite B.

Acknowledgement

The authors thank Professor K. Niihara for providing the research facilities at ISIR, Osaka University, and Professor T. Urabe and Miss K. Saito, Ryukoku University, for the 3D SIA analysis.

References

1. M. RÜHLE, B. J. DALGLEISH and A. G. EVANS, *Scripta Metall.* **21** (1987) 681.
2. G. H. CAMPBELL, M. RUHLE, B. J. DALGLEISH and A. G. EVANS, *J. Am. Ceram. Soc.* **73** (1990) 521.
3. G. PEZZOTTI, K. NODA, Y. OKAMOTO and T. NISHIDA, *J. Mater. Sci.*, **28** (1993) 3080.
4. G. PEZZOTTI, *J. Am. Ceram. Soc.*, **76** (1993) 3323.
5. G. PEZZOTTI, B.-T. LEE, K. HIRAGA and T. NISHIDA, *J. Mater. Sci.*, **28** (1993) 4187.
6. G. PEZZOTTI, *Acta Metall. Mater.*, **41** (1993) 1825.
7. I. TANAKA, G. PEZZOTTI, T. OKAMOTO, Y. MIYAMOTO and M. KOIZUMI, *J. Am. Ceram. Soc.* **72** (1989) 1656.
8. G. PEZZOTTI, I. TANAKA and T. NISHIDA, *Philos. Mag. Lett.*, **67** (1993) 95.
9. M. RÜHLE, A. G. EVANS, R. M. MCMEEKING and P. G. CHARALAMBIDES, *Acta Metall.* **35** (1987) 2701.
10. P. G. CHARALAMBIDES and A. G. EVANS, *J. Am. Ceram. Soc.* **72** (1989) 746.
11. A. KRELL, J. WOLTERSDORF, E. PIPPEL and D. SCHULZE, *Philos. Mag.* **51** (1985) 765.
12. G. PEZZOTTI, I. TANAKA and T. OKAMOTO, *J. Am. Ceram. Soc.* **74** (1991) 326.
13. S. SAKKA, T. SAKAINO, K. TAKAHASHI and N. SOGA in "Glass Handbook" (Asakura Shoten, Tokyo, 1980) p. 657.
14. A. G. EVANS, *Acta Metall.* **26** (1978) 1845.
15. T. MURA and P. C. CHENG, *J. Appl. Mech.* **44** (1977) 591.
16. T. MURA, "Micromechanics of Defects in Solids" (Martinus Nijhoff, The Hague, 1982) p. 66.
17. Z. LI and R. C. BRADT, in "Whisker- and Fiber-toughened Ceramics" (ASM International, USA, 1988) p. 289.
18. T. S. COOK and F. ERDOGAN, *Int. J. Eng. Sci.* **10** (1972) 677.
19. M. C. LU and F. ERDOGAN, *Eng. Fract. Mech.* **18** (1983) 491.
20. J. W. HUTCHINSON, M. E. MEAR and J. R. RICE, *J. Appl. Mech.* **54** (1987) 828.
21. M. Y. HE and J. W. HUTCHINSON, *Int. J. Solids Struct.* **25** (1989) 1053.
22. *Idem. J. Appl. Mech.* **56** (1989) 270.
23. A. K. BHATTACHARYA, J. J. PETROVICH and S. C. DANFORTH, *J. Am. Ceram. Soc.* **75** (1992) 413.
24. A. J. G. OP HET VELD and J. D. B. VELDKAMP, *Fiber Sci. Technol.* **2** (1970) 269.
25. A. GHOSH, M. G. JENKINS, K. W. WHITE, A. S. KOBAYASHI and R. C. BRADT, in "Proceedings of the 3rd International Symposium on Ceramic Materials and Components for Engines" (American Ceramic Society, Las Vegas, 1988) p. 592.

Received 17 December 1992
and accepted 21 September 1993